Mesoscale modelling of concrete under high strain rate tension with a rate-dependent cohesive interface approach

Mesoscale modelling of concrete under high strain rate tension with a rate-dependent cohesive interface approach

Rongxin Zhou [a], Han-Mei Chen [b c]*, Yong Lu [d]

[a] Wolfson School of Mechanical, Electrical and Manufacturing Engineering, Loughborough University, LE11 3TU, UK

[b] Department of Mechanical, Aerospace and Civil Engineering, School of Engineering, The University of Manchester, M13 9PL, UK

[c] School of Architecture, University of Liverpool, L69 7ZN, UK

[d] Institute for Infrastructure and Environment, School of Engineering, The University of Edinburgh, UK

* Correspondence: Hanmei.Chen@liverpool.ac.uk

Abstract

This paper presents the investigation of the dynamic behaviour of concrete material under high strain rate tension using an interface approach in a mesoscale model framework. A rate-dependent cohesive constitutive description is introduced into the mesoscale framework to account for the effects of viscosity occurring in the dynamic fracture process. An algorithm is developed to insert cohesive elements throughout the mesoscale mesh grids in a concrete specimen, and to identify the cohesive element properties based on the original mesoscale structure. After parameter studies in terms of the cohesive element properties, the proposed model is validated against representative experimental data. The model is then employed to

investigate the dynamic tensile behaviour of concrete under high strain rates. The underlying mechanisms of the dynamic tensile strength increase of concrete, including the influence of viscous effect from rate-dependent material description, the inertial effect from cracking and the material heterogeneity, are discussed and identified respectively. Results demonstrate that the viscous effect should be incorporated into the cohesive constitutive law to account for the Stefan effect at low and moderate strain rates and the micro-crack inertial effect only plays a significant role at a relatively high strain rate. Material heterogeneity does influence the strength enhancement under dynamic loading and the significance of this effect increases with the strain rate.

Keywords: concrete material; dynamic tension; heterogeneity; mesoscale model; cohesive element; micro-inertial effect

1. Introduction

The dynamic behaviour of concrete has been a subject of continuous research interest over the last few decades. In concrete structures, the behaviour under dynamic loads is complex due to significant sensitivity of concrete to loading rate. Abundant experimental test data [1–7] show that there is an apparent increase of the dynamic strength and fracture energy, i.e. the so-called dynamic increase factor (DIF), when concrete is subjected to high strain (loading) rates both in compression and tension. However as generally recognized, while the DIF in compression may largely be attributed to the involvement of inertia-induced radial confinement [8–11], the mechanisms behind the increase of the dynamic tensile strength and fracture energy are not clear. Due to the sensitivity of stress conditions to the test setup and the difficulties in accurately measuring the dynamic tensile behaviour of concrete, experimental data under dynamic tensile loading are highly scattered [4,12].

Generally, three indirect methods employing the Hopkinson bar have been developed to investigate the dynamic tensile behaviour of brittle materials like concrete to suit different ranges of the strain rate, namely direct dynamic tensile test, splitting test and spalling test [12,13]. Although all the experimental investigations arrive at the conclusion that there is a definite link between the loading rate and the exhibited response of the specimen, the limitation of the experimental technique itself as well as the composite nature of the concrete material make it very difficult to truly understand the behaviour of concrete under dynamic tension. On this backdrop, high fidelity numerical simulation provides a potentially powerful means to study the influence of individual parameters in great detail.

Up to date, various numerical models which aim to reproduce the experimental setup have been developed to predict the response of concrete under dynamic tensile loading. Cotsovos and Pavlović [14] performed a direct dynamic tension simulation on the concrete prism with a nonlinear rate-independent constitutive model. Based on their results they suggest that the effect of strain rate on the specimen behaviour must be viewed as a structure effect which is directly linked to the axial inertial effect of its mass and the boundary conditions instead of intrinsic material property. More recently, Ožbolt et al. [14–17] conducted a series of numerical simulations to investigate the dynamic fracture of concrete in tension using a microplane constitutive model in which rate dependency is considered to be related to growing micro-cracks and viscosity. Based on the results they proposed that the apparent strength enhancement at relatively high loading rate should consist of two contributions, namely the true material strength which is controlled by the rate-dependent constitutive law and the inertial structure effect which develops automatically from the dynamic response. They also concluded that the results of any indirect tension test such as split Hopkinson bar test need careful interpretation since the apparent strength recorded from experiments may mix up with true material strength and the inertial effect.

On the other hand, Barpi [18] used a viscoplasticity based model, in which a viscosity parameter is defined as a function of strain rate, to describe the dynamic mechanical properties of concrete under splitting test. Their results suggest that viscosity should be the key reason for the increase of DIF in tension. A similar argument has been made by Hentz et al. [19] who developed a 3D discrete element method to simulate the dynamic loading under both compression and tension with Split Hopkinson Pressure Bar. They argued that while the DIF in compression can be largely explained by inertial-based hypothesis (structure effect), the DIF in tension cannot be explained by inertia alone and the rate sensitivity in dynamic tension is more a material intrinsic effect (a material property). Lu and Li [12] simulated three indirect dynamic testing apparatus, direct dynamic tensile test, dynamic splitting test and spalling test by numerical modelling with a homogeneous rate-independent concrete damage model. It was found that the numerical results from these three types of dynamic tensile tests do not show any strain-rate dependency. Hence, they concluded that the strain rate enhancement of the tensile strength observed in dynamic tensile tests is a genuine material effect. They further conducted a qualitative study on a micro-mechanism model and concluded that micro-crack inertia and material property heterogeneity could be the intrinsic mechanisms responsible for DIF. A similar conclusion was also drawn in numerical investigation with a solid-element based mesoscale model [10,20]. It is worth mentioning at this juncture that splitting test has a relatively low valid strain rate limit (1~5 s^{-1}) as beyond this limit the stress distribution would no longer preserve a split tension condition [20].

Mesoscopic numerical simulations on dynamic tension response in concrete were also conducted by many researchers. Zhou and Hao [21] performed a mesoscopic analysis of dynamic behaviour in Brazilian cylinder under splitting tensile loading condition using simplified mesoscale model. It was found that the mesoscopic features like ITZ properties, aggregate positions and aggregate volume fractions can have some influence on the crack

pattern and the measured tensile strength. Erzar and Forquin [22] developed a mesoscopic approach in which the matrix and the randomly distributed aggregates are differentiated to check and validate the accuracy of experimental measurement techniques. Two representative dynamic tensile tests, namely a spalling test and an edge-impact test were both reproduced by numerical simulations. The mesoscopic computational results show good agreement with experimental evidences. Thus, they concluded that the mesoscopic approach can be very useful to validate testing techniques and to simulate the dynamic behaviour of concrete. However, after conducting a series of numerical simulation with a more comprehensive mesoscale concrete model, Lu et al [11,23,24] pointed out that numerical investigation with a solid-element based mesoscale model has inherent limitation in representing a realistic fracture process in concrete specimen, particularly in dynamic loading where the classical mesh-objective treatment of the softening behaviour could cause complications in the propagating stress wave. Consequently, the dynamic tensile strength as well as the dynamic fracture energy could be incorrectly interpreted from the simulation results in such an FE modelling framework.

More recently, several advancent computational methods have also been used to modelling the dynamic fracture in concrete and reinforced concrete, e.g. cracking particles method [25–28] and phase field method [29]. The advantages of these methods rely that complex fracture patterns including crack branching and coalesence can be easily modelled without representation of the crack's topogy and the cracks can be arbirarily orientied. By speicifically, a dynamic cohesive law which takes into account the change of fracture energy under high dynamic loading condition was succesully incoporated into the cracking particle method in [26]. And their results show that the method is capable to represent exprimental data quite accurately for both quasi-static loading and dynamic loading cases.

In summary, despite considerable research effort, questions remain on the various mechanisms behind the dynamic strength increase in concrete materials, especially in quantitative terms. More specifically, the key questions are directed on (i) the significance of different mechanisms in their contribution to the dynamic tensile strength enhancement, and (ii) is it necessary to consider the dynamic tensile strength enhancement in the material constitutive relationship and to what extent does the modelling scale, i.e. the level of details studied, govern the definition of this constitutive relationship? Further exploration of this topic from micromechanical processes that combine the effects of the material heterogeneity, viscosity and micro-crack initiation and propagation is required.

This paper presents an investigation of the dynamic behaviour of concrete material under high strain rate tension using an interface approach in a mesoscale model framework. A rate-dependent cohesive constitutive description is introduced into the mesoscale framework to account for the effects of viscosity in the dynamic fracture process. The paper is organised as follows. In Section 2, a holistic 2D mesoscale model for dynamic fracture is developed, in which cohesive elements are incorporated along all mesh grid lines to accommodate free development of fractures. The numerical model setup and model verification are given in Section 3. In Section 4, the dynamic responses of the concrete specimen and the mechanisms behind these responses are investigated and discussed based on the numerical results. Concluding remarks are presented in Section 5.

2. Modelling approach in a mesoscale framework

2.1 Overview of meso-structure generation

A number of studies on the generation of random meso-structure in concrete specimen both in 2D and 3D can be found in the existing literature [10,11,30]. For the present study on the

dynamic tension of concrete, previous evidences have pointed out that the dynamic inertial confinement, which is of a structure effect nature, has little effect on the DIF in tension [12,18]. More importantly, the present study purposely excludes the structure effect to the contribution of DIF but mainly focus on discussing the intrinsic mechanisms at material level. Therefore, it is considered rational to use a 2D mesoscale model, while the focus is placed on a fuller description of the cohesive features, in addition to the mesoscopic structure of concrete. From a mesoscopic perspective the heterogeneity of concrete has three distinctive phases, i.e., aggregates, mortar matrix and the ITZ. These three phases are explicitly represented in the current mesoscale model. The materials within each phase are considered as homogeneous, although in reality these individual phases, especially mortar and the associated ITZ, are also heterogeneous. Being a sub-mesoscale feature, the non-homogeneous properties within individual phases are expected to play a less significant role in determining the bulk behaviour of concrete.

The general steps in generating a basic 2D meso-structure with aggregates and the mortar matrix follow exactly the approach used in [31,32]. For the cohesive cracking model, the evolved shape of a crack will be dependent upon the initial mesh grids. Although in a mesoscale model the overall shape of a crack may always be captured in a reasonable manner because of the fine mesh resolution needed for the mesoscale structure, triangular elements are preferred so that the detailed crack paths could be simulated more realistically. Figure 1 gives an example of the meshed elements for aggregate and mortar components.

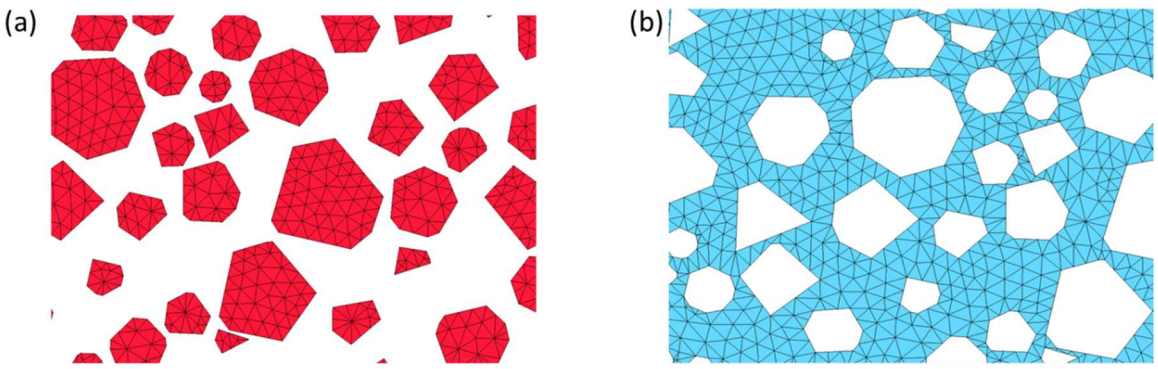

Figure 1 Meso-structure of concrete model (partial region): (a) aggregates; (b) mortar matrix.

2.2 Algorithm for insertion of cohesive interface elements

The fracture mechanism of concrete under dynamic tension is more complex than in static loading. Previous experimental results reveal that cracking is no longer limited to developing in close connection with the ITZ but also runs through mortar matrix and even through the aggregate particles under high strain rate loading [4,33]. Thus, to ensure that a mesoscale model fully capture all possible cracking routes, it is necessary to develop a model with possible discontinuity along all the mesh girds for all three parts, i.e. aggregates, mortar and ITZ.

Depending on the response of the cohesive surface prior to the development into the softening stage, two types of cohesive zone approaches may be considered when the cohesive elements are inserted, namely intrinsic and extrinsic cohesive zone models [25]. Intrinsic cohesive elements are embedded in the discretized structure at the beginning of the simulation, and during the whole simulation process the mesh connectivity remains unchanged. Extrinsic cohesive models, on the other hand, insert the cohesive elements adaptively into the mesh, which means the cohesive elements are inserted only when the boundary stresses reach the critical material strength. Generally, the intrinsic cohesive model allows easier implementation than the extrinsic model as it does not require a constant mesh topology updating which can be complicated and time consuming, although it may introduce some problem in some cases such

as formation of unexpected crack paths and violation of the Cauchy theorem. Moreover, the inserting cohesive element during analysis in extrinsic cohesive model requires that the cohesive strength need to be known a priori, however, the strength at specific material point should also be dependent on the real strain rate at this point. Therefore, it may also bring additional inconvenience for extrinsic cohesive model at dynamic loading analysis. More sophisticated computational methods e.g. cracking particle method [26,27] may be a good candidate to solve this issue, however, this is beyond the scope of the present paper. It is also worth mentioning that potential issues with the intrinsic approach can largely diminish provided that a suitable value is set for the initial stiffness, which will be discussed in detail later. Therefore, in the present study, we adopt the intrinsic cohesive model approach to avoid further complexity in handling the mesoscale mesh during the course of analysis.

In the present mesoscale model with cohesive interface elements, three different types of cohesive elements, namely the aggregate-aggregate (intra-aggregate) interface element, the mortar-mortar (intra-mortar) interface element and the aggregate-mortar interface element can be identified according to the meso-structure of the concrete model. An algorithm is developed for the above-mentioned identification and cohesive element insertion. The procedure is performed with an in-house program coded with MATLAB. The proposed algorithm involves the following steps:

(1) Obtain the nodes and elements files; in the present study these are generated using ANSYS pre-processor;

(2) Read nodal coordinates, element connectivity arrays and then for each existing node i, identify the number of solid elements, n_i, which share this node;

(3) Duplicate nodes. For each original node i, (n_i-1) number of nodes are duplicated with the same coordinates of the node i. Create an array *Nodes[i][j]* to store such duplicated nodes and corresponding original node at the same location, with *j=1* to

n. The original node *i* is stored in *Nodes[i][1]* while the duplicated nodes are stored in *Nodes[i][2]* to *Nodes[i][n]*.

(4) Discretise solid elements. For each original node *i,* loop over the number of solid elements, *n*, sharing this node. The first element using node *i* will keep its nodal connectivity unchanged. However, for the second to the *n*-th solid element, the node *i* in the original connectivity will be replaced by the duplicated *Nodes[i][2]* to *Nodes[i][n]* respectively. This discretising process will be implemented in all the original nodes.

(5) Insert cohesive elements. After updating all the nodal connectivity of the solid elements, all individual solid elements become disconnected units. A zero-thickness interface element is therefore used to connect two adjacent solid elements. This is done using an array *Edges[M][K],* which stores all the edges of the discrete elements, where *M, K* is the element number and the index of edges of this element, respectively. Start with element *M*, edge *K,* which has two end nodes *I* and *J*. Then identify element *N* which has an edge K^* that connects two nodes I^* and J^* with the same locations as nodes *I* and *J,* respectively. Insert one interface element between the two solid elements *M* and *N* with connectivity as $[I, J, I^*, J^*]$. Move to the next edge of element *M* and repeat the same process to insert a new cohesive element. When all edges of element *M* have been dealt with, move to the next element and repeat. Note that if an edge is on the external boundary or has already been dealt with in a previous step, the process will move to the next edge. An example of disconnecting solid elements and inserting a cohesive element between two solid elements is schematically shown in Figure 2.

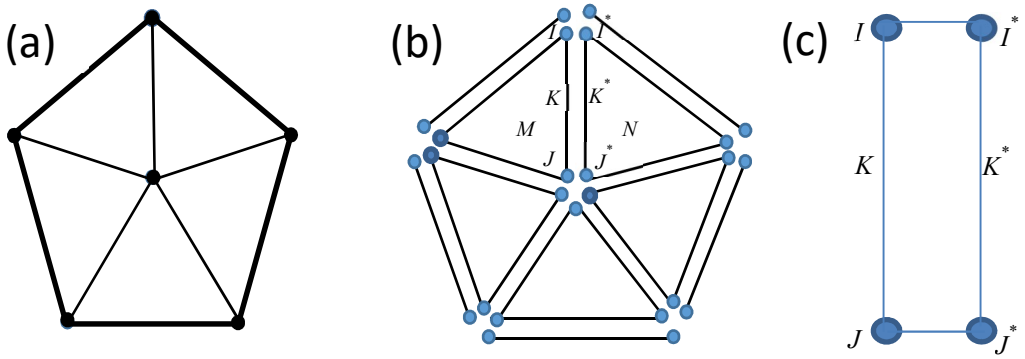

Figure 2 Sketch of inserting cohesive elements in the initial mesh: (a) Initial mesh; (b) disconnecting solid element; (c) forming cohesive element.

(6) Identify material attributions for interface elements. After inserting interface elements along each mesh line, the material type for each interface element needs to be identified according to the meso-structure of the concrete specimen. Firstly, subdivide the element file into three arrays AGG_ELE, MOR_ELE, and INT_ELE, which contain aggregate solid elements, mortar solid elements and the inserted cohesive elements, respectively. Then loop over the number of interface elements stored in the INT_ELE and identify the material type of the cohesive elements one by one. If all nodes of an interface element are shared by a solid element in AGG_ELE, the cohesive element is given the aggregate-aggregate interface properties. Similarly, if all nodes in an interface element are contained by a solid element in MOR_ELE, then the interface elements will be treated as a mortar-mortar interface element. The remaining interface elements, which share part nodes with solid elements in AGG_ELE and part with solid elements in MOR_ELE, will be aggregate-mortar interface elements and will be given the ITZ properties accordingly.

(7) Create the input file for the analysis solver, herein LS-DYNA. Note that the above procedure is implemented based on a 2D plane condition, in which a line with

duplicated nodes is used to model an interface element. However, the cohesive constitutive material model used in LS-DYNA is restricted to 3D solid elements. To cater to this situation, the current 2D mesoscale model is analysed in a thin plate configuration, with a single layer of elements in the out-of-plane direction. Therefore, nodes in this plane are further duplicated to form another plane. The nodes in the original plane and the nodes in the duplicated plane will form 3D solid elements.

Figure 3 shows the insertion and identification process and the results for the three material types of cohesive element.

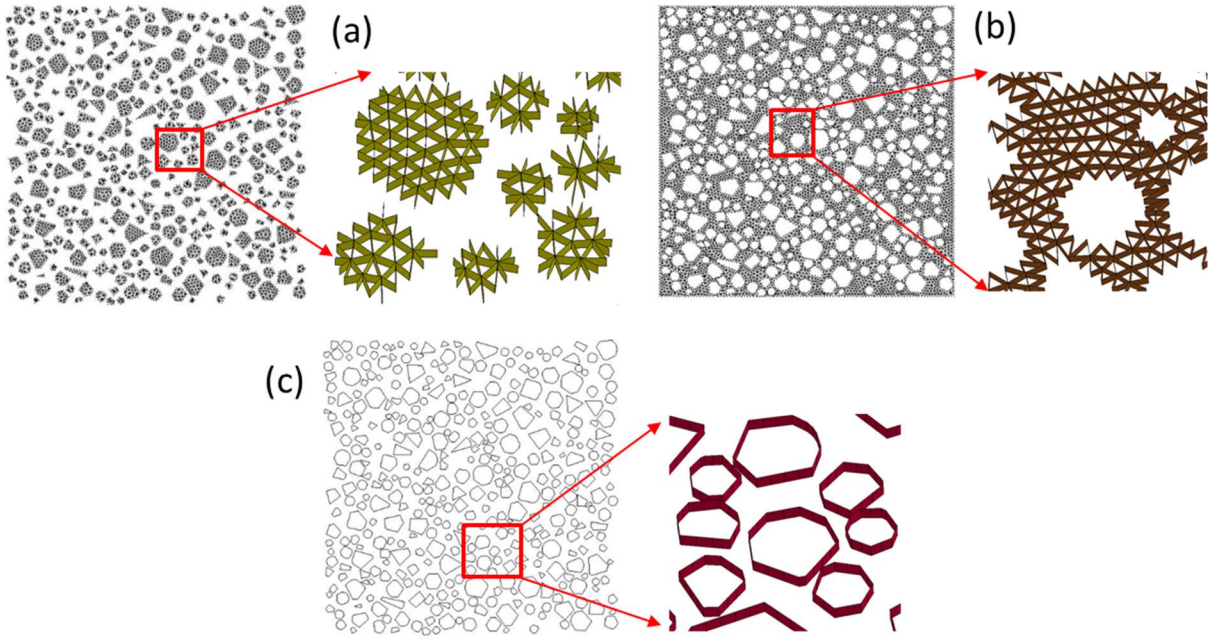

Figure 3 Interface elements for three different components: (a) Aggregate-aggregate interface elements; (b) Mortar-mortar interface elements; (c) Aggregate-mortar interface elements.

2.3 Material models

2.3.1 Cohesive constitutive description

In the present study, we postulate that the cracking procedure as well as the nonlinear behaviour of concrete only develops through fractures, and thus in the model, they are governed by a

constitutive relation between traction and opening displacement in the cohesive elements. The bulk material outside the cohesive zone remains undamaged and it continues to behave linearly elastically. This is to say; a simple linear elastic material model is used for brick element while a nonlinear cohesive constitutive model is adopted for the zero-thickness interface elements. Whereas such a description is broadly consistent with the damage evolution in quasi-brittle material like concrete, it also necessitates a suitable selection of the material constitutive model for the cohesive elements to reproduce reliably the damage processes. A bilinear cohesive constitutive material model used in [11,34,35] is adopted in the present study due to its simple but efficient function. The model considers the irreversible damage and allows for independent definitions of the constitutive relations for different fracture modes of tension and shear (see Figure 4(a)).

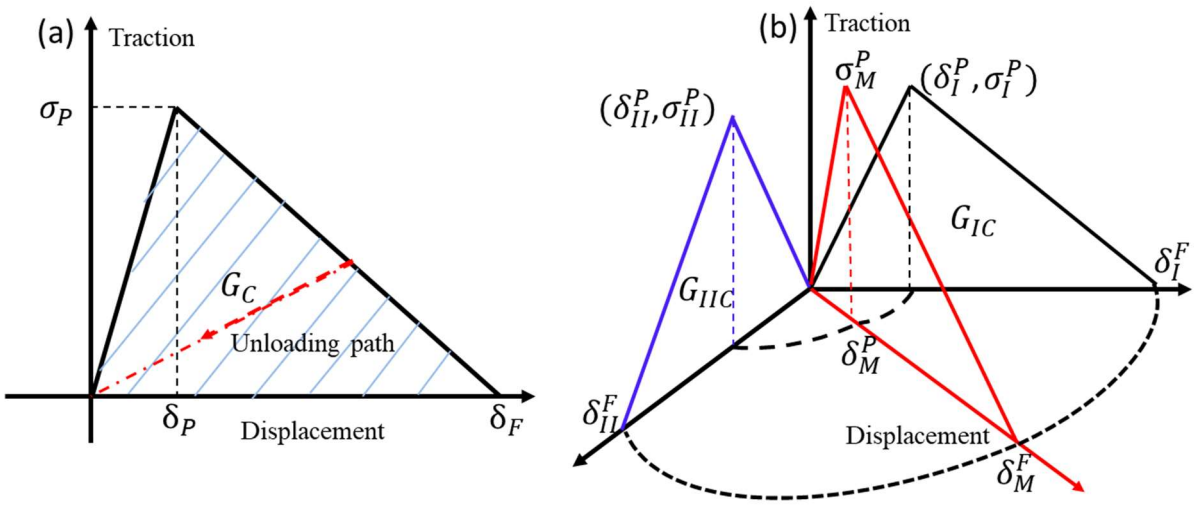

Figure 4 Cohesive constitutive model [30]: (a) in pure mode; (b) in mixed model

The linear stiffness of the bilinear cohesive model is defined as σ_P/δ_P , and this is followed by a linear softening during the damage (post-peak). Thus, a simple relationship exists between the energy release rate G_C, the peak traction σ_P, and the ultimate displacement (at zero traction) δ_F as:

$$G_C = \sigma_P \times \delta_F / 2. \quad (1)$$

The cohesive model can also simulate the complex fracture behaviour by combining normal and shear traction components together. As suggested by Gerlach et al [36], the detailed coupling between two independent modes may be described as shown in Figure 4(b). $\sigma_I^P, \sigma_{II}^P$ and σ_M^P are the pure mode-I, the pure mode-II and the mixed-mode traction when fracture initiates and δ_I^P, δ_{II}^P, δ_M^P are their corresponding displacement respectively. The displacement in pure mode-I, pure mode-II and mixed-mode when cohesion is completely lost (the interface is separated) are denoted by $\delta_I^F, \delta_{II}^F, \delta_M^F$ respectively. G_{IC} and G_{IIC} are the fracture energy release rate in mode-I and mode-II respectively. The detailed coupling law between independent mode-I and Mode-II fractures can be found in [37].

2.3.2 A rate-dependent cohesive law

A rate-independent cohesive interface model combining with contact-friction approach has been successfully incorporated into the mesoscale framework in [11] for the material investigation as well as characterisation of the material behaviour in complex loading conditions. However, a rate-dependent cohesive constitutive description is required in the framework to account for the effects of viscosity occurring during the dynamic fracture process of concrete.

The rate-dependent tractions for tension and shear fracture model of the cohesive element may be expressed by a liner logarithmic function [38]:

$$T\left(\dot{\varepsilon}\right) = T_0 + T_1 \left\langle \ln \frac{\dot{\varepsilon}_{eq}}{\dot{\varepsilon}_{0T}} \right\rangle \text{ and } S\left(\dot{\varepsilon}\right) = S_0 + S_1 \left\langle \ln \frac{\dot{\varepsilon}_{eq}}{\dot{\varepsilon}_{0S}} \right\rangle, \quad (2)$$

where $\dot{\varepsilon}_{0T}$, $\dot{\varepsilon}_{0S}$ are the reference strain rates, T_0 and S_0, are the tractions at reference loading rate for pure mode-I, pure mode-II respectively. T_1 and S_1 are material parameters which are used to calibrate the rate-dependent model. Angle bracket ⟨ ⟩ in Eq. (2) denotes Dirac delta

function which has the definition as: $\langle f \rangle = f$ if $f > 0$ and 0 otherwise. The equivalent strain rate $\dot{\varepsilon}_{eq}$, for mixed-mode fracture, in the interface element can be evaluated as [38]:

$$\dot{\varepsilon}_{eq} = \frac{\sqrt{\dot{u}_T^2 + \dot{u}_S^2}}{t_{element}}, \tag{3}$$

where $\dot{u}_T$ and $\dot{u}_S$ represent the local separation speed of the interface layer in normal and tangential direction respectively and $t_{element}$ refers to the thickness of the interface. It should be noted here $t_{element}$, the thickness of the interface, is the current separation distance of the initial interfaces and is calculated based on the current nodal coordinates.

In the present cohesive constitutive law, the fracture energy under dynamic loading can also be defined as a function of the equivalent strain rate $\dot{\varepsilon}_{eq}$. However, to avoid the complexity, we restrained ourselves on studying the DIF for tensile strength only, the fracture energy enhancement for the fracture energy is not considered although it was also observed from experimental evidences. Moreover, many researchers (e.g.[23,25]) also stated that the fracture energy enhancement during dynamic tensile loading should come from multiple cracks and wider region of damage zone (structural effect) instead of from material constitutive description. In this circumstance, the fracture energy is set to be rate-independent at material constitutive description.

3. Model set up and experimental verification

3.1 Specimen geometry and loading method

A typical cubic concrete specimen (a square in 2D) with a side length equal to 100 mm is considered herein for the basic model verification. The aggregate volume ratio in the specimen is approximately 45%, and the maximum aggregate size is 8 mm. To simulate a direct tension,

the sample specimen is loaded using a linear velocity distribution as shown in Figure 5. The lateral boundaries are kept stress-free and no boundary condition is imposed in the out-of-plane direction, such that a macroscopic 1D stress state prevails in the structure.

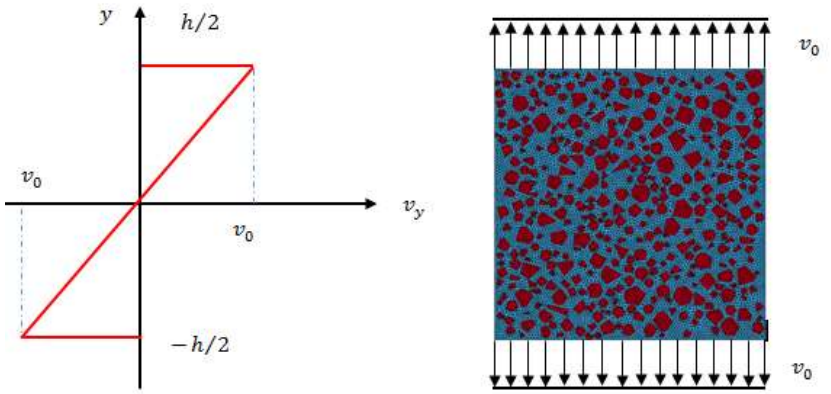

Figure 5 Boundary conditions for dynamic tension

It should be noted at this juncture that under a high strain rate it is very difficult to achieve a homogenous stress distribution in a concrete specimen under dynamic tensile loading. In the present study with a numerical simulation, a special treatment is used to avoid stress wave reverberation and an early failure near the boundary, such that all nodes in the FE model are given a velocity in accordance with a prescribed distribution along the specimen length, as shown in Figure 5. This approach has been adopted in some previous studies as well [25,35]. For a linear distribution of velocity, we have:

$$v(y) = \frac{2v_0}{h} y, \tag{4}$$

where v_0 is the loading velocity applied on the upper and lower boundary of the specimen and its value is dependent on the imposed strain rate $\dot{\varepsilon}$

$$v_0 = \dot{\varepsilon} \frac{h}{2}. \tag{5}$$

h and y are the height (length) of the specimen and the vertical coordinate value of the nodes, respectively.

3.2 Mesh size and initial cohesive stiffness

The mesh size could have a significant influence on the global response of the concrete specimen since it monitors the amount, size and orientation of cohesive elements. General convergent value has been obtained in quasi-static loading cases (e.g. [11]). However, the response of concrete in dynamic loading is more complex due to the involvement of the stress wave as well as the crack propagation speed, thus the numerical results may be more sensitive to the element size. For these reasons, numerical tests with different mesh sizes under various loading rates are performed to investigate the mesh size effect and seek for an effective mesh size in the dynamic loading cases. Figure 6(a) and (b) shows the convergence results for tensile loadings under two different strain rates, namely, quasi-static loading and strain rate 100 s^{-1}, in terms of nominal stress-strain curve. In the present study, the nominal stress is calculated as the upper boundary loading force divided by the initial width while the nominal strain is determined from the displacement on the upper boundary divided by the half height of the specimen due to symmetric loading conditions and the nominal strength refers to the peak value of nominal stress. To eliminate any influence introduced by the initial stiffness of the cohesive element while ensuring minimum artificial compliance of intrinsic cohesive element [39], a constant but sufficiently large stiffness $K_N = K_S = 2\times10^7$ MPa / mm is used for all the cases. From Figure 6(a), using a mesh grid size of 1 mm appears to be good enough even for a high strain rate of 100 s^{-1}. Therefore, the mesh size 1 mm has been used as the final mesh setting thereafter, resulting in around resulting in about 140k nodes and 70k elements including 30k bulk elements and 40k interface elements, respectively for the mesoscale model.

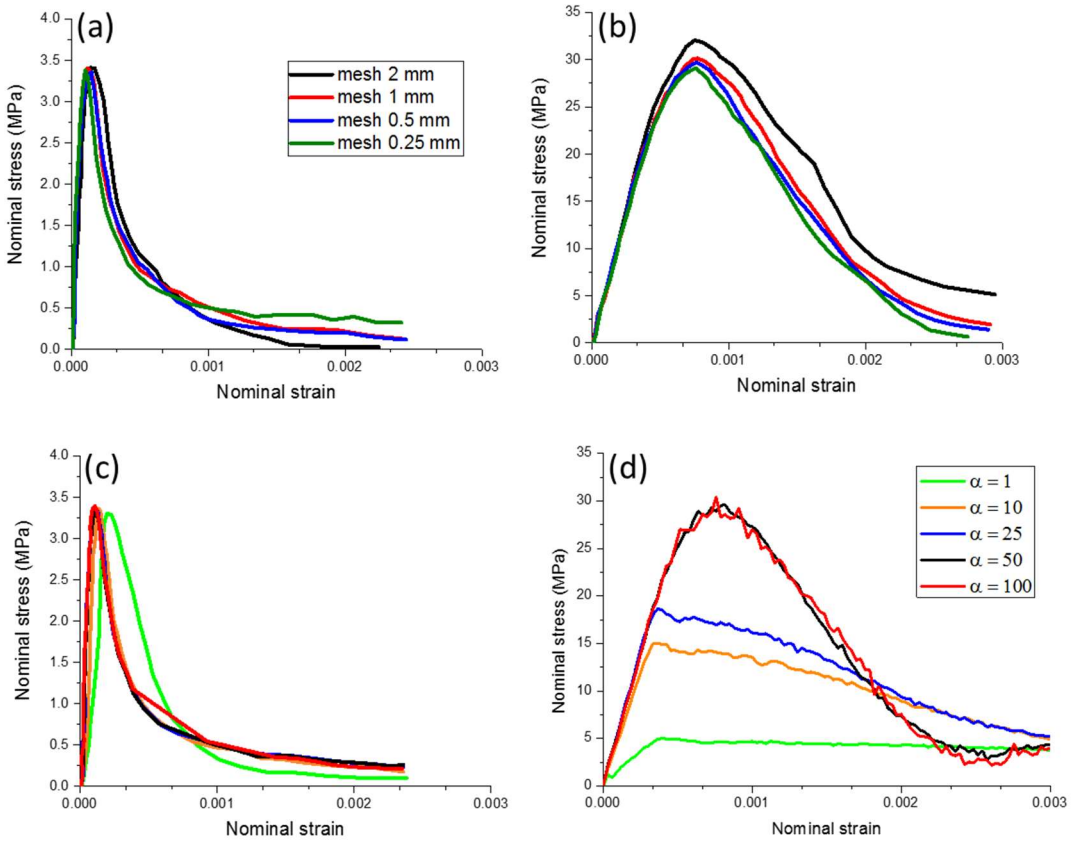

Figure 6 Effect of mesh size and initial cohesive stiffness: (a) mesh size study at quasi-static loading; (b) mesh size study at high strain rate loading 100 s^{-1} ; (c) initial cohesive stiffness at quasi-static loading; (d) initial stiffness at high strain rate loading 100 s^{-1}.

The initial stiffness for the intrinsic cohesive element can be a very important parameter which may influence the global response of the cohesive zone model [11,39]. While the small value of the initial stiffness may introduce artificial compliance, an extremely large stiffness may cause other numerical problems such as spurious oscillations of the traction and increase of the computational time. A general guideline for this parameter may be expressed by the following equation [39]:

$$K = \frac{\alpha E}{h_{mesh}}, \tag{6}$$

where E is Young's modulus of the bulk material, h_{mes} is the element mesh size in the cohesive zone, and α is the stiffness parameter which needs to be determined. Eq. (6) also implies that the stiffness of the cohesive element may be set appropriately only after the mesh size is determined.

In [11], the suggested value of parameter α is around 50 which is deemed to be a sufficient value to reduce the compliance of the intrinsic cohesion in quasi-static loading cases. This conclusion is further checked herein for dynamic loading cases. For this purpose, the computed results in term of nominal stress and strain in a high strain rate loading condition (100 s^{-1}), with various values of α for the mesh size 1 mm are presented in Figure 6(b). From Figure 6(b), it can be found that the initial cohesive stiffness not only influences the global stiffness of the nominal stress-strain curve but can also affect the dynamic strength in the high loading rates. However, the use of a value $\alpha = 50$ for the stiffness parameter appears to guarantee a stable and converging result.

3.3 Model calibration and verification

The meso-mechanical approach requires defining the material properties for every constituent material component. As described earlier, the bulk elements in the concrete specimen should resemble the continuum properties before cracking, while the cohesive elements accommodate the fracture (damage) process. Therefore, the bulk elements are modelled only with a simple linear elastic material model while the zero-thickness cohesive element is assigned with a bilinear cohesive constitutive relation in terms of traction and opening displacement. The basic material properties for the aggregates and the mortar matrix are summarised in Table 1. These values are generic and suitable for a normal concrete with a static tensile strength on the order of 3.5 MPa [40].

Table 1 Properties for the bulk element

Component	Density $\boldsymbol{\rho}$ (kg/mm^3)	Young's modulus E (GPa)	Poisson's ratio v
Aggregate	2600	60	0.2
Mortar	2300	30	0.2

The setting of the material parameters in the bilinear cohesive constitutive model can be very simple and straightforward. Only a few key parameters, including the initial stiffness K_N, K_S, the peak traction σ_I^P, σ_{II}^P, and the fracture energy release rate G_{IC} and G_{IIC} in mode-I and mode-II respectively, need to be identified. While the peak traction σ_I^P and the fracture energy G_{IC} in Mode-I can be directly obtained from representative experiments for most engineering materials, the corresponding values in the shear direction may need extensive parameter studies for a specialised material due to a lack of the relative experimental data. In the present study, the material properties in tension for the three independent interface components are directly determined on the basis of experimental data (e.g. [41,42]) taking into consideration of the suggested values from previous numerical work (e.g. [40]). The shear properties for the three independent interfaces are set according to the studies in [11] where the shear strength and the shear fracture energy are reported to be 4 times of tensile strength and 10 times of the tensile fracture energy respectively. According to their report, with such setting for the two factors, the numerical model can give good agreement with the experimental evidences for both global stress-strain curve and local damage patterns. In order to keep consistent description of the rate-dependent responses of the three components (aggregate-aggregate, mortar-mortar and aggregate-mortar), the rate-dependent parameters T_1 and S_1 are set directly related with their counterparts in quasi-static loading. Then the Eq. (2) and can be written as:

$$T\left(\dot{\varepsilon}\right) = T_0 + k_1 T_0 \left\langle \mathrm{In}\frac{\dot{\varepsilon}_{eq}}{\dot{\varepsilon}_{0T}} \right\rangle \text{ and } S\left(\dot{\varepsilon}\right) = S_0 + k_1 \left\langle \mathrm{In}\frac{\dot{\varepsilon}_{eq}}{\dot{\varepsilon}_{0S}} \right\rangle. \tag{7}$$

Notice that the same k_1 is used in both mode-I and mode-II because of the proportional relation between tensile and shear description in quasi-static loading case. Taking consideration of the DIF values for tensile strength from experimental observation for concrete, several simulations were then conducted to calibrate the value of k_1. The results show that a value around 1 appears to give very satisfied results for all the loading rates. Therefore, Therefore, Eq. (2) can be transformed to:

$$\frac{T(\dot{\varepsilon})}{T_0} = 1 + \left\langle \ln \frac{\dot{\varepsilon}_{eq}}{\dot{\varepsilon}_{0T}} \right\rangle \text{ and } \frac{S(\dot{\varepsilon})}{S_0} = 1 + \left\langle \ln \frac{\dot{\varepsilon}_{eq}}{\dot{\varepsilon}_{0T}} \right\rangle. \tag{8}$$

This rate-dependent cohesive law is then adopted, hereafter, for all the cohesive models.

The properties of the ITZ layer are difficult to determine precisely. Past research has found that the thickness associated with the ITZ in concrete is generally in the range of 20-50 μm [43,44]. An exact incorporation of such a thin layer of material in the mesoscale FE model is impractical. Therefore, it is reasonable to use zero-thickness cohesive elements to represent the interface as we actually did in the present study.

Similar with interphase zone in the polymeric composites [45], the ITZ in concrete plays a crucial role in determining the macroscopic failure behaviour of concrete. An adequate representation of the ITZ is an important subject in the mesoscale model. Lots of work have been conducted on investigating the effect of ITZ mechanical properties on the fracture behaviour of concrete-like materials [11,34,44]. And it is generally accepted that the ITZ is weaker and is about 50% of the strength of the mortar matrix. All the mechanical properties for ITZ including the strength and fracture energy are determined based on data collected from relevant literatures [25,46] and our previous sufficient work [11,31].

The detail material parameter values used for the three different interfaces are summarised in Table 2. One may also note that the properties of ITZ in the present study are set at 50% of the mortar properties as generally accepted.

Table 2 Properties for the three interface components

Component	Tensile strength σ_I^P (MPa)	Fracture energy G_{IC} (N/mm)	Shear strength σ_{II}^P (MPa)	Fracture energy G_{IIC} (N/mm)
Aggregate-aggregate	16	0.08	64	0.8
Mortar-mortar	4.7	0.06	18.8	0.6
Aggregate-mortar	2.3	0.03	9.2	0.3

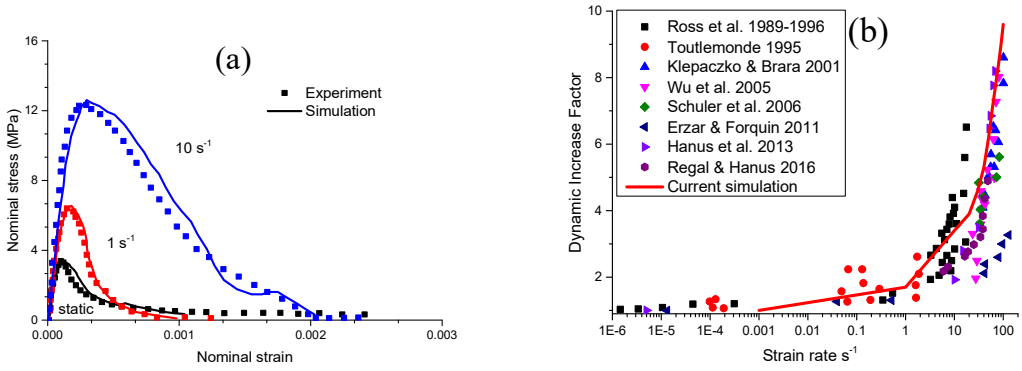

Figure 7 Model verification with experimental results: (a) stress-strain curves verified with [47]; (b) DIF with strain rate towards experimental evidences collected from [48]

As can be seen from Figure 7(a), the results from the mesoscale cohesive element model show very good overall agreement with the experimental data in terms of stress-strain curves under three different strain rates, namely, 10^{-3} s^{-1}, 1 s^{-1} and 10 s^{-1}. Furthermore, more simulations are conducted at various loading rates range from 10^{-3} s^{-1} to 100 s^{-1} to extract the dynamic increase factor (DIF). As can be seen from Figure 7 (b), a reasonable correlation between the experimental DIF with strain rate curves and the numerical predictions for all the loading rates

is achieved. From these comparisons, it is reasonable to say that the mesoscale cohesive element model has the capability to predict the response of concrete under dynamic tensile loadings with acceptable accuracy. Therefore, the model is further applied in the analysis of intrinsic mechanisms governing the dynamic strength enhancement in dynamic tension, which will be given in Section 4.

4. Numerical investigation of mesoscale mechanisms influencing tensile behaviour of concrete

4.1 General dynamic response in concrete

As stated earlier, concrete materials are very sensitive to the strain rate, especially in tension. However, the mechanisms behind its global dynamic behaviour are not clear, and debates are still ongoing as to whether it is a material effect or a structure effect, and if both what is the relative significance between these effects. Some researchers [16] also stated that the results of any indirect tension test, such as split Hopkinson bar test, may mix up with structure effect and material effect, thus need a more careful interpretation. However, it should be noted that the structural inertial effect described above is purposely excluded from the present analysis by introducing a specified loading condition as described in Section 3.1. Examination of the response is focused within the mesoscale parts of the model.

To facilitate the evaluation of the stress distribution, the mesoscale region is fictitiously divided into seven equal strips along with the loading (axial) direction, with a width around 14 mm for each strip. This way, the thin direction of the strip is aligned with the loading direction, as depicted in Figure 8.

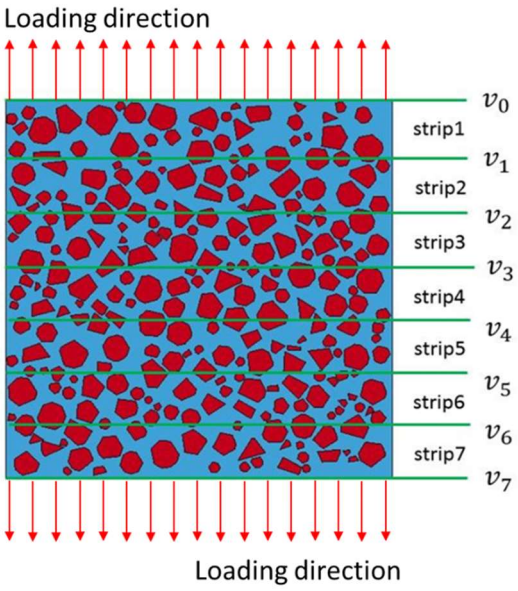

Figure 8 Strips to evaluate the stress distribution in the specimen

Figure 9 shows the development of (average) axial stress in the seven strips for the above three strain rates respectively along with the corresponding final cracking patterns. The stresses in all the strips show almost the same response under each strain rate. This tends to confirm that a relatively uniform stress state could be achieved for all the loading rates under the artificial loading condition, thus precluding the structural inertial effect from the numerical analysis. Hence, if there exhibits any strength enhancement with the increase of strain rate, the mechanism should come from the material effect in terms of the rate sensitivity of the cohesive behaviour rather than the structural effect. Actually, as shown in Figure 9, the dynamic strengths obtained from the present numerical simulations show a significant increase when higher strain rates are imposed. Since the structural inertial effect has been effectively excluded, the observed dynamic strength enhancement is attributable only to the intrinsic material response. Other structural effects that may influence the dynamic strength of concrete, like the structural size of the specimen, are also purposely avoided. The numerical specimen size used in the presently study is at the same level with typical experimental tests and is exact the same in all the simulations. Moreover, according to the recent study in [49], the dynamic tensile

strength will be independent on the structural size of the specimen when the imposed strain rate is above the critical strain rate 1 s^{-1}. Since the present study mainly focus on investigating the dynamic tensile behaviour at relative high strain rate (above 1 s^{-1}), it is reasonable to believe that the effect of structural size on our results is very tiny and can be neglected.

Three mechanisms at the material level, namely material heterogeneity, material viscosity and the micro-crack inertial effects, are included in the current mesoscale cohesive numerical model. Therefore, the observed dynamic tensile strength enhancement (i.e. the DIF) from the numerical results is a result of their combined action. To further demonstrate the individual contribution to the DIF from each of the above three mechanisms, more specific investigations are carried out in the following sub-sections.

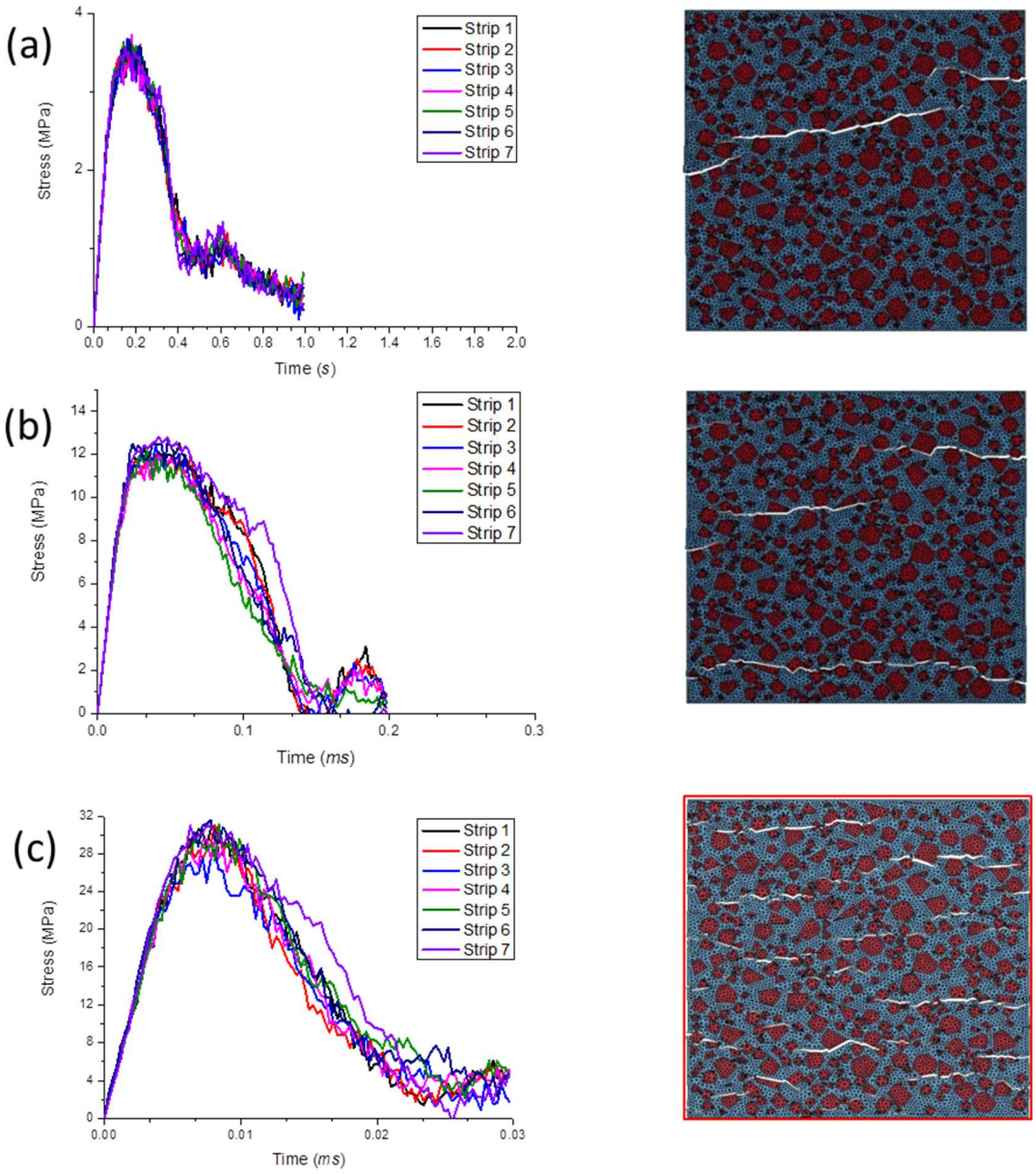

Figure 9 Strip stresses and crack patterns under different loading rates: (a) at strain rate 10^{-3} s^{-1}; (b) at strain rate 10 s^{-1}; (c) at strain rate 100 s^{-1}

4.2 Effect of rate-dependent material response

To examine the effect of rate sensitivity at the material constitutive property level, numerical simulations in this section are performed using both a rate-independent cohesive model and the proposed rate-dependent cohesive model. In the rate-independent cohesive model, the cohesive

strength and the fracture energy for both tension and shear model are set as constants regardless of the strain rate. All other aspects of the models remain identical.

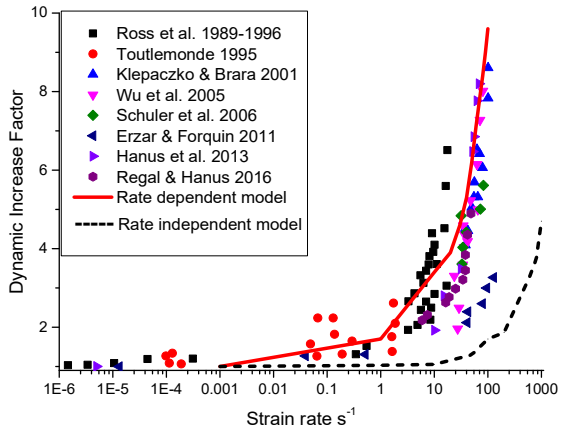

Figure 10 Comparison of DIF with strain rate between rate-independent cohesive and rate-dependent cohesive models

The corresponding results are compared in Figure 10 in terms of DIF with strain rate curves. As can be clearly observed, at the range of low and intermediate strain rates (up to 10 s^{-1}), nearly no strength enhancement can be observed from the rate-independent cohesive model, which is contrary to the experimental evidences. The discrepancy could come from the 'Stefan effect' which is not incorporated in the rate-independent cohesive model. The 'Stefan effect' refers to a viscous phenomenon which takes place in the capillary pores [50,51]. This phenomenon can be simply interpreted by pulling apart two plates separated by a thin water film. The force necessary to pull the plates apart increases with the increase of the loading speed. Apparently, explicit modelling of the 'Stefan effect' would require a representation of free water content and reflection of complex physical interaction between moisture and micro-structural solid skeleton [51,52], which are not within the remit of current mesoscale concrete model. In addition, for all the loading rates, the mesoscale rate-independent cohesive model generally lacks ability to reproduce the dynamic responses observed from experimental evidences. Therefore, it is reasonable to conclude that it is necessary to incorporate the rate-

dependent constitutive law at the material level to account for the 'Stefan effect' and its interaction with other mechanisms.

However, results of DIF at higher strain rates (above 10 s^{-1}) demonstrate that rate- independent cohesive model can also predict remarkable dynamic strength enhancements, especially for the very high strain rate range (above 100 s^{-1}), even no rate effect is considered at the material level. And this strength enhancement should come from other micro-mechanisms, such as material heterogeneity and micro-crack inertial effect, which will be discussed in the following sub-sections.

4.3 Effect of material heterogeneity

To investigate the effect of heterogeneity on the DIF, a comparative homogenous FE model i.e. homogeneous cohesive elements (HC model) is analysed in this section, along with the mesoscale model. For the homogeneous model, the bulk elements (mortar and aggregates) are homogenised with uniform material properties, whereas the zero-thickness interface element with homogenized properties is inserted between each pair of bulk elements. Similar to the original mesoscale cohesive element model (MC model), only a simple linear elastic material model is employed for the bulk elements, and the nonlinear and cracking behaviour are represented by the cohesive constitutive material model. The homogenization process is conducted at quasi-static loading case only and it is expected that HC model can predict the same results with MC model in terms of stress-strain curve at quasi-static loading case. For bulk element in the HC model, the material parameter needed to be homogenized is just the Young's modulus E_{Ho} since a simple liner elastic material model is used. For cohesive element, the parameters used for homogenization are the tensile strength $\overline{\sigma_I^p}$ and the fracture energy $\overline{G_I}$, while other properties including the shear properties and the rate-dependent

parameters can be set directly related with these two values. The methodology used for homogenization can be referred in [53,54]. After homogenization, the values of E_{Ho}, $\overline{\sigma_I^p}$ and $\overline{G_I}$ in HC model are 43.5 GPa, 3.2 MPa, 0.05 N/mm, respectively.

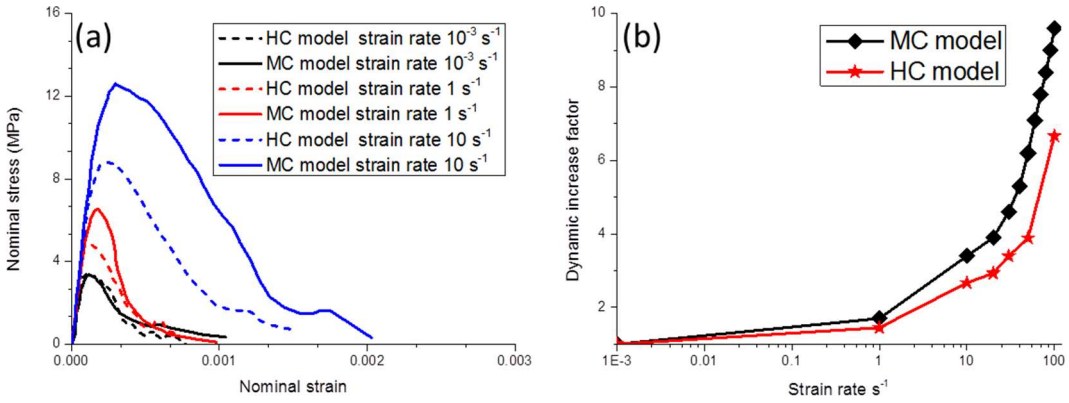

Figure 11 Effect of material heterogeneity: (a) nominal stress-strain curves; (b) DIF with strain rate

The results in terms of the stress-strain curve and the DIF with strain rate curves from the two models are shown in Figure 11. As can be seen, the stress-strain response in quasi-static (i.e. 10^{-3} s^{-1}) is very similar in HC and MC model, which also indicates that the successful homogenisation of the MC model to the HC model. However, when the loading rate increases to a moderate strain rate of 10 s^{-1}, the nominal strengths in the mesoscale cohesive model (MC) show larger increases in the dynamic strength as compared with its counterpart in the homogeneous model (HC). As the loading rate further increases, much larger differences of nominal strengths between MC and HC models can be observed (e.g. at a strain rate of 100 s^{-1}). This suggests that the material heterogeneity of concrete plays a more significant role under high strain rate loading.

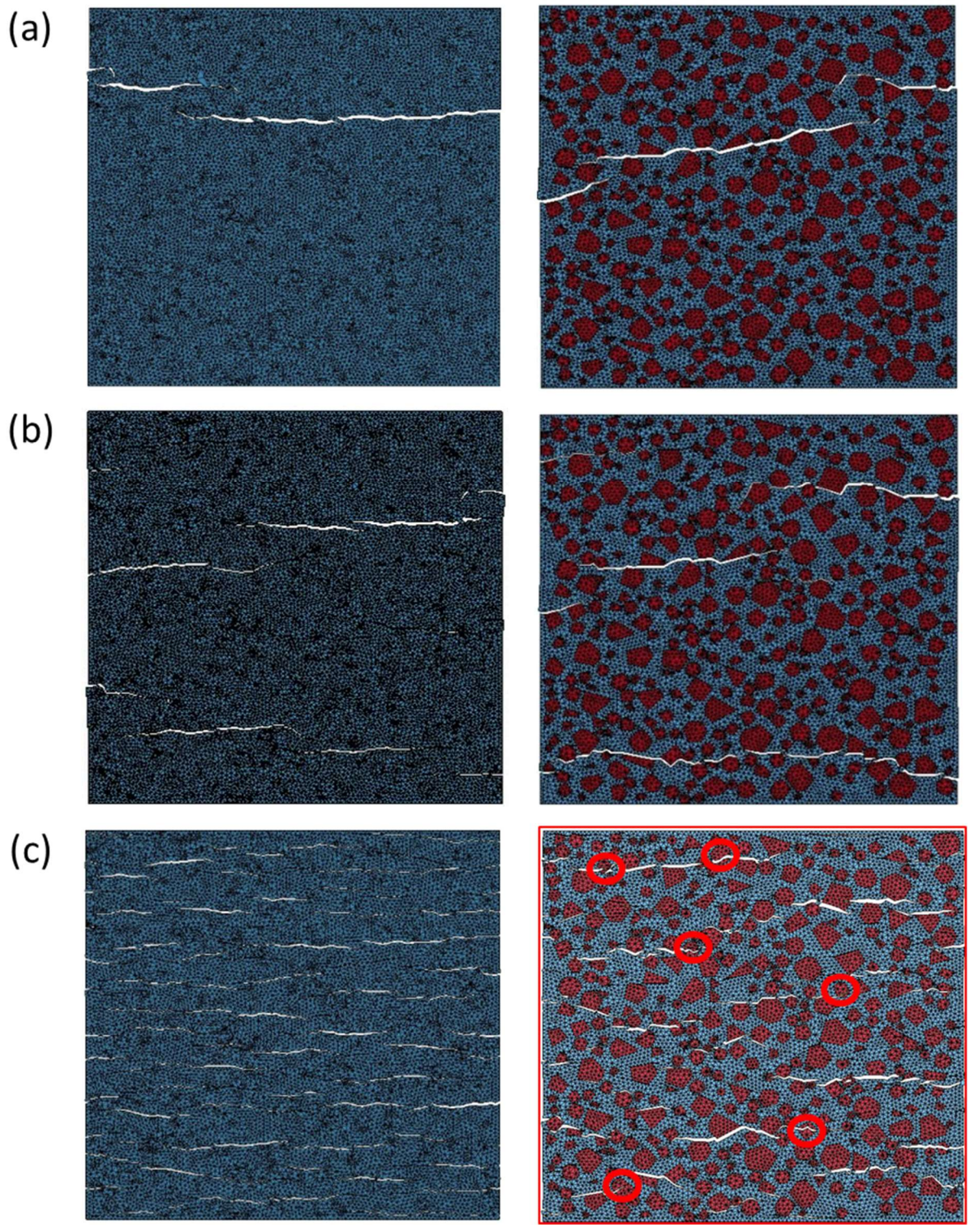

Figure 12 Final cracked patterns for HC (left) and MC (right) models: (a) at quasi-static test; (b) at strain rate 10 s^{-1}; (c) at strain rate 100 s^{-1}

The final crack patterns for HC and MC models under various loading rates are compared in Figure 12. Due to the special loading methodology used in current simulations, it may be very difficult to make a direct comparison with the experimental evidences. However, typical characteristics of crack patterns of concrete are successfully captured by our current mesoscale cohesive model. It can be seen clearly that the cracks in the mesoscale cohesive model exhibit more wavy paths compared with the corresponding homogeneous model. Furthermore, from the failure patterns in the mesoscale cohesive model, cracks mostly propagate around the aggregate particles and following the interface between the mortar and aggregate particles at lower strain rate loading; however, under high strain rates (e.g. 100 s^{-1}) some cracks penetrate through the aggregates, as can be seen from Figure 12(c). The fracture of aggregate particles thus contributes to the increase of the tensile strength as well as fracture energy, especially under high strain rate loading. This statement echoes well relevant experimental evidences (e.g.[48,55]).

Having clarified the general contribution of the material heterogeneity in the dynamic tensile behaviour of concrete, further analysis is performed to examine the relative importance of the rate sensitivity of the three constituent materials, i.e. ITZ, mortar, and aggregates respectively. For this purpose, three variant models are created, and in each model, only one set of the cohesive elements, representing (a) ITZ, (b) mortar, and (c) aggregate, respectively, are made rate dependent. To assess the individual contribution to the DIF from each component in a mesostructured concrete, a variable called relative contribution is defined and calculated as:

$$RC^{(I)} = \frac{\left(f_d^{(I)} - f_s\right)/f_s}{\sum\left(f_d^{(I)} - f_s\right)/f_s}, \tag{9}$$

where f_s is the static tensile strength of the studied concrete, $f_d^{(I)}$ refers to the predicted dynamic strength when rate effect cohesive constitutive law is considered only in one

component and the superscript *I* represents individual component in the mesoscale concrete i.e., aggregate, mortar and ITZ respectively.

It should be noted here there is no physical meaning for the variable $RC^{(I)}$; it is defined and used only for characterisation of the relative role of each component in a mesostructured concrete.

The relative contribution of DIF for all three components are quantified at three strain rates, namely, 1 s^{-1}, 10 s^{-1} and 100 s^{-1}, represents low strain rate, moderate strain rate and high strain rate loading, respectively. The corresponding results are shown in Figure 13. It is interesting to find that the relative effect of the mesostructured component varies with the increase of the loading rate. Generally, ITZ plays a significant role in the strength enhancement while the aggregate nearly contributes nothing to the strength enhancement at low strain rate. This phenomenon is very similar to the quasi-static loading test where the load-carrying capacity of concrete is largely controlled by the weaker ITZ [10,11]. However, with the increase of the strain rate, aggregate particles tend to play an increasingly more important role in the strength enhancement. When the strain rate increases to the order of 100 s^{-1}, a remarkable contribution from aggregate particles can be observed. This echoes the observation in Figure 12(c), where several aggregate particles were fractured by cracks, thus contributing to the strength enhancement. In contrast, mortar always has a high contribution to the DIF at any strain rate in the range of loading. This may be because mortar is more compliant than aggregate and fracture and damage in concrete mainly occurs in the mortar component for both quasi-static and dynamic loadings.

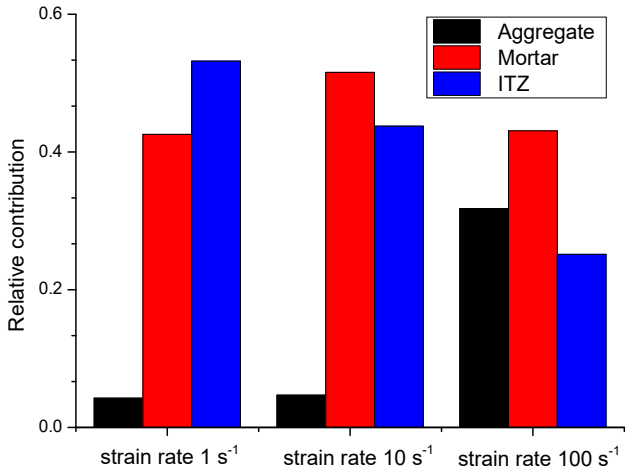

Figure 13 Relative contributions of mesoscale components under different strain rates

4.4 Effect of micro-crack inertia

In Section 4.2, it was observed that under high strain rates (100 s^{-1} and above), marked strength enhancement occur even in the rate in-dependent cohesive model. This phenomenon could be attributable to the micro-inertial effect. A further discussion of this micro-crack inertial effect is presented in this section. The investigation is based on the comparison of the numerical results between the mesoscale finite element model with cohesive interface elements (MC model) and a mesoscale model with only solid elements (i.e. without cohesive interface elements). The latter model is denoted as mesoscale solid element model (MS model), and as it does not involve an explicit fracture, the micro-inertia is considered to be minimal.

To make a direct comparison, the MS and MC models use exactly the same meso-structure and the mesh size. Furthermore, no DIF is pre-imposed at the material constitutive level for both models to exclude the viscous effect. In the model with the cohesive elements (MC model), the nonlinear response is represented only by the cohesive constitutive model (MAT_138 in LS-DYNA) while the bulk elements are modelled by simple linear elastic properties. In the solid element model (MS model), the K&C concrete damage model (MAT_72R3 in LS-DYNA) is

employed which simulates the macroscopic response of concrete. This K&C concrete damage model is capable of describing the material failure due to tension, shear, as well as compression under various stress conditions. The detailed technical information about this material model can be found in [10,56]. The material model has been tested extensively and is found to be a suitable candidate for quasi-static as well as dynamic applications of concrete-like materials [31]. The implementation of this material model is very easy as only the uniaxial compressive strength is required to input and other parameters have been already calibrated well to give standard stress-strain curve for target class of concrete. The MC and MS models are considered to be equivalent at quasi-static loading case as they predict very similar results in terms of stress-strain curve. To avoid any bias parameterization, the material properties setting including the tensile strength and fracture energy for the three individual components are at the same level for the two models. The input compressive strength in the MS model for the three components, namely the aggregate, mortar and ITZ, are 150 MPa, 45 MPa and 23 MPa, respectively. These give the three components have the value of tensile strength and fracture energy in mode-I, around 16 MPa, 0.08 N/mm, 4.7 MPa, 0.06 N/mm, and 2.3 MPa, 0.03 N/mm [31,56], respectively.

Figure 14(a) shows the dynamic tensile strength enhancement for the above models. Very little dynamic strength enhancement can be observed from the MS model for all the loading rates. On the other hand, for the MC model, although the strength enhancement is very limited at the strain rate up to 100 s^{-1}, the DIFs show very steep increase when the loading rate further increases; and as can be observed from Figure 14(a), the DIF value reaches around 5 at strain rate of 1000 s^{-1} for the MC model.

The underlying difference between the cohesive element model and the solid element models is that the cohesive element model can explicitly simulate the initiation and propagation of cracks through the time-dependent cohesive interfaces (see Figure 14(b)). The damage of the

cohesive element model initiates when the traction reaches a criterion established in term of the traction but the fracture process is usually controlled by the fracture toughness which is a measure of the energy required for a crack to grow. This means a crack can only propagate when the fracture energy release rate reaches a critical value G_c. Therefore, the cohesive constitutive law incorporating with the critical energy release rate introduces a length scale, named cohesive zone length l_{cz} into the material description [25,57]. The cohesive theories, in addition to building a characteristic cohesive zone length into the material description, endow the cohesive constitutive behaviour with an intrinsic time scale in terms of the longitudinal wave speed and the cohesive material parameters. The cohesive model exhibits different mechanic response when subjected to fast and slow loading rates due to this intrinsic time scale. This gives the cohesive model an ability to predict rate-dependent crack initiation time and crack propagation speed in brittle solids, so that the dynamic strength enhancement on strain rate can be accounted. Therefore, it is reasonable to postulate that the dynamic resistance increase obtained from the cohesive element models is mainly due to the micro-crack inertial effect on initiation and propagation from micro-mechanic mechanism.

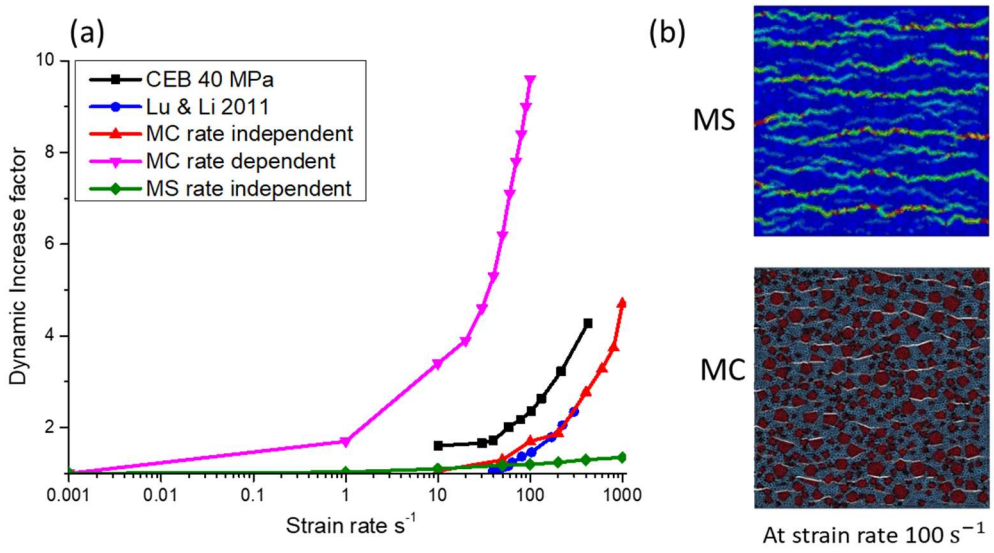

Figure 14 Comparisons between MS model and MC model: (a) DIF with strain rate towards data collected from [12,58]; (b) damage (crack) pattern

It is worth mentioning here that a qualitative analysis conducted in [59], suggested that the micro-crack inertial effect on dynamic strength enhancement can only occur beyond a loading rate $\dot{\sigma} = 5000\ \mathrm{GPa/s}$ ($\dot{\varepsilon} \approx 150\ /\mathrm{s}$) in a concrete material with the maximum aggregate size $d_{aggr} = 10\ \mathrm{mm}$ and tensile strength $f_t = 3\ \mathrm{MPa}$ when a longitudinal wave speed $C_r = 1800\ \mathrm{m/s}$ is considered. Lu and Li [12] conducted a similar qualitative analysis based on micro-mechanism model and demonstrated that micro-crack inertia is one of the mechanisms responsible for the increase of the dynamic tensile strength with strain-rate observed in the dynamic tensile tests on concrete-like materials. From their results, the DIF curves as a function of strain rate can be separated into two parts. For strain rate up to the order of 100 s^{-1}, the DIF grows slowly with the increase of the strain rate. But, when the strain rate is beyond 100 s^{-1}, the DIF increases rapidly. This is consistent with the conclusion in [59] that the micro-crack inertial effect can only dominate the apparent rate dependency of the tensile strength at a relatively high strain rate. The numerical results in the present study well reproduce this tendency with the cohesive element models. As shown in Figure 14, the DIFs curves calculated from our mesoscale rate-independent cohesive model agree very well with the theoretic predictions and steep increments of the DIFs can only be observed at relative higher strain rate, i.e. above 100 s^{-1}.

Other micro mechanisms behind the dynamic strength enhancement phenomenon could come from the multiple micro-cracks interaction and coalescence in the concrete specimen [34,35]. It can be observed from the cracking patterns in Figure 12 that the number of cracks increases when the loading rate increases. A single major crack can be observed at the quasi-static loading test, whereas multiple cracks in a distributed manner occur in the specimen at a higher strain rate of the order of 100 s^{-1}. The transition from a single crack to distributed cracks has a strong influence on the macroscopic behaviour of the concrete. The local stress state is modified around these micro-cracks by a stress-relief wave propagating on both sides of a crack.

The rapid release of microscopic tensile stress in the vicinity of the existing micro-cracks acts to delay the coalescence of the cracks in the interaction zone, resulting in an increase of the peak strength.

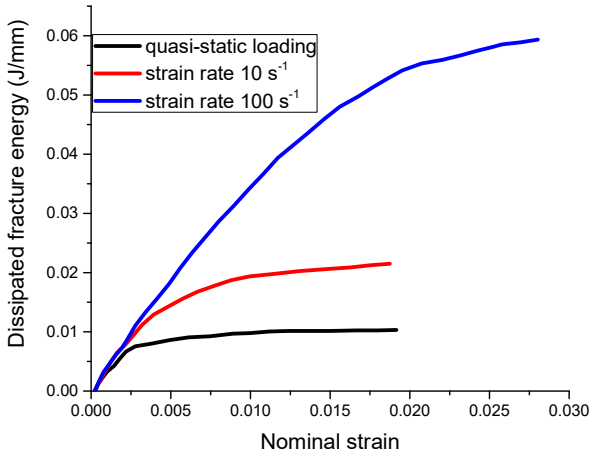

Figure 15. Evolution of dissipated fracture energy under different strain rate loading.

Figure 15 shows the dissipated fracture energy time histories for MC model under various strain rate loading. the dissipated fracture energy strongly depends on the loading rate even with a rate independent local fracture energy at material level. This may also support our hypothesis that unlike the tensile strength enhancement, the higher fracture energy during dynamic tensile loading is purely a structural effect, which comes from diffuse micro-cracking and wider regions of damage zone.

One may also notice that crack branching, which is a typical crack pattern of concrete under dynamic loading, is not captured in current simulations. The reason may result from the special loading methodology used in the mesoscale cohesive models. As can be seen from the crack patterns in Figure 12, the model with such a loading methodology has already predicted multiple cracks under high strain rate loading. The initiation, propagation and their interactions

of the multiple cracks will significantly release the stress filed and fracture energy in front of each crack-tip. Therefore, the crack branching is largely prohibited in current simulations.

5. Conclusions

In this paper, a holistic 2D mesoscale cohesive element model is developed, in which cohesive elements are incorporated between all interfaces between the bulk elements. This approach enables an explicit simulation of the crack initiation and propagation in the concrete specimen along the ITZ as well through the bulk elements. Moreover, the model allows the use of simple constitutive description of the bulk materials while nonlinear behaviour is achieved by the cohesive and cracking behaviour through the cohesive elements. As such, the classical mesh-related problems in a continuum-based model for cracking are largely reduced, making the model highly suitable for investigation of cracking behaviour for both quasi-static and dynamic applications. It should be noted the mesh-dependency cannot be fully eliminated since cracks necessarily have to follow the mesh edges, but can be drastically reduced if the mesh is very fine.

An algorithm has been developed to insert cohesive element throughout the mesh grids in a concrete specimen and to identify the cohesive element properties based on the original mesoscale structure.

The validated model is employed to investigate the dynamic tensile behaviour under high strain rates and the influences of key parameters including the viscous effect from rate-dependent cohesive constitutive law, material heterogeneity and micro-inertia effects. Based on the parametric results, the following specific conclusions may be drawn:

1. The dynamic increase of the tensile strength of concrete is found to be attributable to several important factors, and these include cracking through the cohesive mechanism

and the micro-inertia effect associated with cracking; viscous effect from rate-dependent constitutive law; and the material heterogeneity.

2. It is necessary to incorporate the rate-dependent cohesive constitutive law at the material level to account for the 'Stefan effect' and its interaction with other mechanisms, especially at low and moderate strain rates loading.

3. The material heterogeneity does influence the dynamic response of the concrete, and this influence becomes increasingly significant with the increase of the strain rate.

4. The intrinsic time scale, which is incorporated in the cohesive constitutive model, enables the cohesive model to simulate the micro-crack inertial effect on the crack initiation and propagation, which manifests as a rate enhancement of the dynamic strength on the strain rate. Such a rate-sensitive mechanism tends to be activated in the present mesoscale cohesive model at a relatively high strain rate in the order of 100 /s. This observation supports the general argument from past studies that there exists a transition of rate-sensitivity which divides the DIF curve into two distinctive segments.

At present the numerical platform has been realised in 2D mesoscale model. In principle the algorithm can be easily extended to 3D, and by doing so both realistic 3D stress environment and explicit representation of the fracture processes can be accommodated in a unified framework, allowing for numerical investigation in a further broadened spectrum of problems with concrete structures. Of course, such a complete 3D mesoscale with explicit fracture process capabilities will pose much increased demand on the computational cost, and in this respect enhancement in the computational efficiency will require dedicated research.

Declaration of Competing Interest

The authors whose names listed in this manuscript certify that there is NO actual or potential conflict of interest in relations to this article.

References

[1] Grote DL, Park SW, Zhou M. Dynamic behavior of concrete at high strain rates and pressures: I. experimental characterization. Int J Impact Eng 2001;25:869–86. doi:10.1016/S0734-743X(01)00020-3.

[2] Klepaczko JR, Brara A. An experimental method for dynamic tensile testing of concrete by spalling. Int J Impact Eng 2001;25:387–409. doi:10.1016/S0734-743X(00)00050-6.

[3] Schuler H, Mayrhofer C, Thoma K. Spall experiments for the measurement of the tensile strength and fracture energy of concrete at high strain rates. Int J Impact Eng 2006;32:1635–50. doi:10.1016/J.IJIMPENG.2005.01.010.

[4] Weerheijm J, Van Doormaal JCAM. Tensile failure of concrete at high loading rates: New test data on strength and fracture energy from instrumented spalling tests. Int J Impact Eng 2007;34:609–26. doi:10.1016/J.IJIMPENG.2006.01.005.

[5] Jin X, Hou C, Fan X, Lu C, Yang H, Shu X, et al. Quasi-static and dynamic experimental studies on the tensile strength and failure pattern of concrete and mortar discs. Sci Rep 2017;7:15305. doi:10.1038/s41598-017-15700-2.

[6] Forquin P, Lukić B. On the Processing of Spalling Experiments. Part I: Identification of the Dynamic Tensile Strength of Concrete. J Dyn Behav Mater 2018;4:34–55. doi:10.1007/s40870-017-0135-1.

[7] Lukić BB, Saletti D, Forquin P. On the Processing of Spalling Experiments. Part II: Identification of Concrete Fracture Energy in Dynamic Tension. J Dyn Behav Mater 2018;4:56–73. doi:10.1007/s40870-017-0138-y.

[8] Li QM, Meng H. About the dynamic strength enhancement of concrete-like materials in

a split Hopkinson pressure bar test. Int J Solids Struct 2003;40:343–60. doi:10.1016/S0020-7683(02)00526-7.

[9] Zhou XQ, Hao H. Modelling of compressive behaviour of concrete-like materials at high strain rate. Int J Solids Struct 2008;45:4648–61. doi:10.1016/J.IJSOLSTR.2008.04.002.

[10] Zhou R, Song Z, Lu Y. 3D mesoscale finite element modelling of concrete. Comput Struct 2017;192:96–113. doi:10.1016/J.COMPSTRUC.2017.07.009.

[11] Zhou R, Lu Y. A mesoscale interface approach to modelling fractures in concrete for material investigation. Constr Build Mater 2018;165:608–20. doi:10.1016/J.CONBUILDMAT.2018.01.040.

[12] Lu YB, Li QM. About the dynamic uniaxial tensile strength of concrete-like materials. Int J Impact Eng 2011;38:171–80. doi:10.1016/j.ijimpeng.2010.10.028.

[13] Forquin P, Riedel W, Weerheijm J. Dynamic test devices for analyzing the tensile properties of concrete. Underst Tensile Prop Concr 2013:137-181e. doi:10.1533/9780857097538.2.137.

[14] Cotsovos DM, Pavlović MN. Numerical investigation of concrete subjected to high rates of uniaxial tensile loading. Int J Impact Eng 2008;35:319–35. doi:10.1016/J.IJIMPENG.2007.03.006.

[15] Ožbolt J, Bošnjak J, Sola E. Dynamic fracture of concrete compact tension specimen: Experimental and numerical study. Int J Solids Struct 2013;50:4270–8. doi:10.1016/J.IJSOLSTR.2013.08.030.

[16] Ožbolt J, Sharma A, İrhan B, Sola E. Tensile behavior of concrete under high loading rates. Int J Impact Eng 2014;69:55–68. doi:10.1016/J.IJIMPENG.2014.02.005.

[17] Ožbolt J, Bede N, Sharma A, Mayer U. Dynamic fracture of concrete L-specimen: Experimental and numerical study. Eng Fract Mech 2015;148:27–41. doi:10.1016/J.ENGFRACMECH.2015.09.002.

[18] Barpi F. Impact behaviour of concrete: a computational approach. Eng Fract Mech 2004;71:2197–213. doi:10.1016/J.ENGFRACMECH.2003.11.007.

[19] Hentz S, Donzé F V., Daudeville L. Discrete element modelling of concrete submitted to dynamic loading at high strain rates. Comput Struct 2004;82:2509–24. doi:10.1016/J.COMPSTRUC.2004.05.016.

[20] Lu Y. Modelling the dynamic response of concrete with mesoscopic heterogeneity. Underst Tensile Prop Concr 2013:218-272e. doi:10.1533/9780857097538.2.218.

[21] Zhou XQ, Hao H. Mesoscale modelling of concrete tensile failure mechanism at high strain rates. Comput Struct 2008;86:2013–26. doi:10.1016/J.COMPSTRUC.2008.04.013.

[22] Erzar B, Forquin P. Analysis and modelling of the cohesion strength of concrete at high strain-rates. Int J Solids Struct 2014;51:2559–74. doi:10.1016/J.IJSOLSTR.2014.01.023.

[23] Lu Y, Xu J, Weerheijm J. A mesoscale modelling perspective of cracking process and fracture energy under high strain rate tension. 2013.

[24] Lu Y, Zhou R. Holistic mesoscale modelling of concrete – Recent developments. Proc. 14th Int. Conf. Comput. Plast. - Fundam. Appl. COMPLAS 2017, vol. 2017- Janua, 2017.

[25] Snozzi L, Caballero A, Molinari JF. Influence of the meso-structure in dynamic fracture simulation of concrete under tensile loading. Cem Concr Res 2011;41:1130–42. doi:10.1016/J.CEMCONRES.2011.06.016.

[26] Rabczuk T, Zi G, Bordas S, Nguyen-Xuan H. A simple and robust three-dimensional cracking-particle method without enrichment. Comput Methods Appl Mech Eng 2010;199:2437–55. doi:10.1016/J.CMA.2010.03.031.

[27] Rabczuk T, Belytschko T. A three-dimensional large deformation meshfree method for

arbitrary evolving cracks. Comput Methods Appl Mech Eng 2007;196:2777–99. doi:10.1016/J.CMA.2006.06.020.

[28] Rabczuk T, Belytschko T. Cracking particles: A simplified meshfree method for arbitrary evolving cracks. Int J Numer Methods Eng 2004;61:2316–43. doi:10.1002/nme.1151.

[29] Ren HL, Zhuang XY, Anitescu C, Rabczuk T. An explicit phase field method for brittle dynamic fracture. Comput Struct 2019;217:45–56. doi:10.1016/J.COMPSTRUC.2019.03.005.

[30] Wang XF, Yang ZJ, Yates JR, Jivkov AP, Zhang C. Monte Carlo simulations of mesoscale fracture modelling of concrete with random aggregates and pores. Constr Build Mater 2015;75:35–45. doi:10.1016/J.CONBUILDMAT.2014.09.069.

[31] Tu Z, Lu Y. Mesoscale modelling of concrete for static and dynamic response analysis -Part 1: model development and implementation. Struct Eng Mech 2011;37:197–213. doi:10.12989/sem.2011.37.2.197.

[32] Zhou R, Chen H-M. Mesoscopic investigation of size effect in notched concrete beams: The role of fracture process zone. Eng Fract Mech 2019;212:136–52. doi:10.1016/J.ENGFRACMECH.2019.03.028.

[33] Brara A, Klepaczko JR. Experimental characterization of concrete in dynamic tension. Mech Mater 2006;38:253–67. doi:10.1016/J.MECHMAT.2005.06.004.

[34] Zhou W, Zhao C, Liu X, Chang X, Feng C. Mesoscopic simulation of thermo-mechanical behaviors in concrete under frost action. Constr Build Mater 2017;157:117–31. doi:10.1016/J.CONBUILDMAT.2017.09.009.

[35] Saksala T. Numerical modelling of concrete fracture processes under dynamic loading: Meso-mechanical approach based on embedded discontinuity finite elements. Eng Fract Mech 2018;201:282–97. doi:10.1016/J.ENGFRACMECH.2018.07.019.

[36] Gerlach S, Fiolka M. Modelling and analysis of adhesively bonded joints with interface elements for crash analysis. LS- 2005:35–44.

[37] Zhou R, Rongxin. Mesoscopic analysis of damage mechanisms in concrete material. The University of Edinburgh, 2016. doi:https://www.era.lib.ed.ac.uk/handle/1842/23650.

[38] Marzi S, Hesebeck O, Brede M, Kleiner F. A rate-dependent cohesive zone model for adhesively bonded joints loaded in mode i. J Adhes Sci Technol 2009;23:881–98. doi:10.1163/156856109X411238.

[39] Turon A, Dávila CG, Camanho PP, Costa J. An engineering solution for mesh size effects in the simulation of delamination using cohesive zone models. Eng Fract Mech 2007;74:1665–82. doi:10.1016/J.ENGFRACMECH.2006.08.025.

[40] López CM, Carol I, Aguado A. Meso-structural study of concrete fracture using interface elements. I: numerical model and tensile behavior. Mater Struct 2008;41:583–99. doi:10.1617/s11527-007-9314-1.

[41] Elices M, Rocco C, Roselló C. Cohesive crack modelling of a simple concrete: Experimental and numerical results. Eng Fract Mech 2009;76:1398–410. doi:10.1016/J.ENGFRACMECH.2008.04.010.

[42] Rosselló C, Elices M, Guinea GV. Fracture of model concrete: 2. Fracture energy and characteristic length. Cem Concr Res 2006;36:1345–53. doi:10.1016/J.CEMCONRES.2005.04.016.

[43] Nitka M, Tejchman J. Modelling of concrete behaviour in uniaxial compression and tension with DEM. Granul Matter 2015;17:145–64. doi:10.1007/s10035-015-0546-4.

[44] Scrivener KL, Crumbie AK, Laugesen P. The interfacial transition zone (ITZ) between cement paste and aggregate in concrete. Interface Sci 2004;12:411–21. doi:10.1023/B:INTS.0000042339.92990.4c.

[45] Msekh MA, Cuong NH, Zi G, Areias P, Zhuang X, Rabczuk T. Fracture properties prediction of clay/epoxy nanocomposites with interphase zones using a phase field model. Eng Fract Mech 2018;188:287–99. doi:10.1016/J.ENGFRACMECH.2017.08.002.

[46] Camacho GT, Ortiz M. Computational modelling of impact damage in brittle materials. Int J Solids Struct 1996;33:2899–938. doi:10.1016/0020-7683(95)00255-3.

[47] Cadoni E, Solomos G, Albertini C. Concrete behaviour in direct tension tests at high strain rates. Mag Concr Res 2013;65:660–72. doi:10.1680/macr.12.00175.

[48] Régal X, Hanus JL. Experimental Study of the Dynamic Flexural Strength of Concrete. Exp Mech 2017;57:427–42. doi:10.1007/s11340-016-0243-1.

[49] Jin L, Yu W, Du X, Yang W. Dynamic size effect of concrete under tension: A numerical study. Int J Impact Eng 2019;132:103318. doi:10.1016/J.IJIMPENG.2019.103318.

[50] Ross CA, Tedesco JW, Kuennen ST. Effects of Strain Rate on Concrete Strength. ACI Mater J 1995;92:37–47. doi:10.14359/1175.

[51] Pedersen RR, Simone A, Sluys LJ. Mesoscopic modeling and simulation of the dynamic tensile behavior of concrete. Cem Concr Res 2013;50:74–87. doi:10.1016/J.CEMCONRES.2013.03.021.

[52] Pedersen RR, Simone A, Sluys LJ. An analysis of dynamic fracture in concrete with a continuum visco-elastic visco-plastic damage model. Eng Fract Mech 2008;75:3782–805. doi:10.1016/J.ENGFRACMECH.2008.02.004.

[53] Durr N, Sauer M, Hiermaier S. A numerical study on mesoscale simulation of quartzite and sandstone under shock loading. Int J Impact Eng 2017;108:73–88. doi:10.1016/J.IJIMPENG.2017.04.008.

[54] Durr N, Sauer M, Hiermaier S. Mesoscale investigation of dynamic fracture in quartzite and sandstone and homogenization to macroscale. Int J Solids Struct 2018;144–

145:160–79. doi:10.1016/J.IJSOLSTR.2018.04.024.

[55] Vegt I, Breugel V, Weerheijm J. Failure mechanisms of concrete under impact loading. 2007.

[56] Magallanes JM, Wu Y, Javier Malvar L, Crawford JE. 1 th International LS-DYNA ® Users Conference Recent Improvements to Release III of the K&C Concrete Model. n.d.

[57] Ruiz G, Pandolfi A, Ortiz M. Three ‐ dimensional cohesive modeling of dynamic mixed ‐ mode fracture. Int J Numer Methods Eng 2001;52:97–120. doi:10.1002/nme.273.

[58] Ceb-Fip, MC90 C. Ceb-Fip Model Code 1990 1993. doi:10.1680/ceb-fipmc1990.35430.

[59] Weerheijm J, Forquin P. Response mechanisms of concrete under impulsive tensile loading. Underst Tensile Prop Concr 2013:181–217. doi:10.1533/9780857097538.2.181.